Communication

Schottky-barrier-free contacts with two-dimensional semiconductors by surface-engineered MXenes

Yuanyue Liu, Hai Xiao, and William A. Goddard

J. Am. Chem. Soc., **Just Accepted Manuscript** • DOI: 10.1021/jacs.6b10834 • Publication Date (Web): 22 Nov 2016

Schottky-barrier-free contacts with two-dimensional semiconductors by surface-engineered MXenes

Yuanyue Liu[1,2*], Hai Xiao[1], William A. Goddard III[1*]

[1]Materials and Process Simulation Center, [2]The Resnick Sustainability Institute, California Institute of Technology, Pasadena, California 91125, United States

Supporting Information Placeholder

ABSTRACT: Two-dimensional (2D) metal carbides and nitrides, called MXenes, have attracted great interest for applications such as energy storage. Here we demonstrate their potential as Schottky-barrier-free metal contacts to 2D semiconductors, providing a solution to the contact-resistance problem in 2D electronics. Based on first principles calculations, we find that the surface chemistry strongly affects the Fermi level of MXenes: O termination always increases the work function with respect to that of bare surface, OH always decreases it, while F exhibits either trend depending on the specific material. This phenomenon originates from the effect of surface dipoles, which together with the weak Fermi level pinning, enable Schottky-barrier-free hole (or electron) injection into 2D semiconductors through van der Waals junctions with some of the O-terminated (or all the OH-terminated) MXenes. Furthermore, we suggest synthetic routes to control the surface terminations based on the calculated formation energies. This study enhances the understanding of the correlation between surface chemistry and electronic/transport properties of 2D materials, and also gives practical predictions for improving 2D electronics.

TEXT MXenes are a class of two-dimensional (2D) metal carbides/nitrides that have the general formula of $M_{n+1}X_nT_x$ (where M is an early transition metal, X is C and/or N, T represents a surface terminating group, and n = 1 to 3)[1-3]. They are usually produced by selective etching of the A element layer from the bulk $M_{n+1}AX_n$ phases[4] (where A = Al, Si etc.), using strong etching solutions such as HF or a mixture of HCl and LiF[1, 2, 5]. This process leads to T = O, OH, and/or F. The layers are then exfoliated by sonication[1, 2, 5]. MXenes have already shown a great potential in batteries[6-9], capacitors[5, 10, 11], and water treatment[12, 13].

Many MXenes have excellent electrical conductivity, which benefits their use as electrodes in electrochemical systems.[1, 2] Here we demonstrate their potential as Schottky-barrier-free metal contacts to 2D semiconductors. Although electronics based on 2D semiconductors (e.g. transition metal dichalcogenides, black phosphorus) have attracted great interest, their development is significantly hindered by the large Schottky barrier (SB) at the metal-semiconductor junction (MSJ).[14-16] Very recently, the use of Ti_2CT_x as electrodes for 2D MoS_2 and WSe_2 field effect transistors have been experimentally demonstrated, yet with significant SBs[17]. Here we predict that SB-free contacts can be achieved by using MXenes with proper surface terminations, which form van der Waals (vdW) junctions[16, 18, 19] with 2D semiconductors. We also suggest synthetic routes to control the surface termination based on the calculated formation energies.

We focus here on MXenes that have already been experimentally realized or have available MAX precursors[4]. We performed Density Functional Theory (DFT) calculations using the Vienna Ab-initio Simulation Package (VASP)[20, 21] with projector augmented wave (PAW) pseudopotentials[22, 23] and the Perdew–Burke–Ernzerhof (PBE) exchange-correlation functional[24]. In some cases, we also used the B3PW91 hybrid functional[25] (which is more accurate but computationally expensive) for comparison. The London Dispersion (vdW attraction) interactions in the heterojunction are corrected using the empirical D3 method[26]. We used 400 eV for the plane-wave cutoff, and fully relaxed the systems until the final force on each atom is less than 0.01 eV/Å.

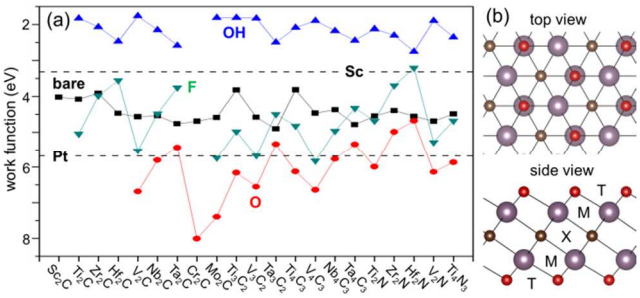

Figure 1. (a): work functions of MXenes with various terminations. Bare surface: black square; O termination: red circle; OH: blue up-triangle; F: cyan down-triangle. For comparison, the work functions of Sc and Pt metal are indicated by dashed lines. (b): atomic structure of a representative M_2XT_2. M: purple; X: gray; T: red.

Figure 1b shows a representative structure of an MXene. The M and X layers alternate following ABC close packing, and T prefers to be on the *fcc* site of the surface to maximize the coordination with M (the exceptions are group-6 MXenes, Cr_2CT_x and Mo_2CT_x, whose stacking depends on T; see Supporting Information (SI) for details). Here we first consider that all surface sites are occupied by one type of T (the case of mixed T will be discussed later). Fig. 1a shows the calculated work function (W) for various MXenes. Note that some of them are semiconductors (Sc_2CO_2, $Sc_2C(OH)_2$, Sc_2CF_2, Ti_2CO_2, Hf_2CO_2, Zr_2CO_2, $Cr_2C(OH)_2$, and Cr_2CF_2), the W of which is not an intrinsic property but rather depends on the doping and hence is not shown. The W of some of the MXenes has been calculated in Ref.[27], which agrees with our results. We find that W is sensitive to T: compared with bare surface, O termination always increases W, OH always decreases W, while F exhibits either trend depending on the specific material.

Interestingly, all the OH terminated MXenes have a rather low W, even lower than that of Sc metal, which has been reported to have a small SB with multilayer MoS_2[28]. Some of the O terminated MXenes have a rather high W, even higher than that of Pt metal, which has the highest W among the elemental metals. The W of F terminated MXenes (W_F) always falls between the corresponding W_O and W_{OH}. In addition, we observe a positive correlation between W_F and W_O, but a negative correlation between W_{OH} and W_O. These correlations become clear in **Figure 2**a, where W_F and W_{OH} are plotted against W_O.

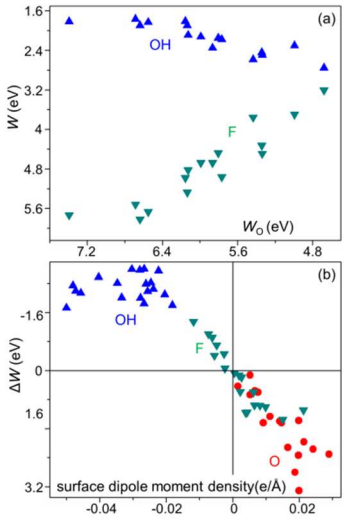

Figure 2. (a) Work function of OH and F terminated MXenes as a function of the work function of O terminated MXenes. (b) Work function variation induced by surface termination, as a function of surface dipole moment density (see the main text for definition).

To understand these observations, we partition the W of a T terminated MXene (W_T) as:

$$W_T = W_{bare} + \Delta W = W_{bare} + C{\cdot}\Delta D_s + \Delta E_F, \quad (1)$$

where ΔW is the change in W with respect to that bare surface (W_{bare}), ΔD_s is the change of surface dipole moment density induced by T, C is a constant, and ΔE_F is the Fermi level shift due to the chemical bonding between T and M. The ΔD_s is generally defined as:

$$\Delta D_s = \int_{z1}^{z2}\iint z\Delta\rho(x,y,z)\mathrm{d}x\mathrm{d}y/S \quad (2)$$

where $\Delta\rho$ is the change of charge density (including ions that can be treated as point charges) induced by T, z is the coordinate normal to the surface, and S is the surface area. $\Delta\rho$ gradually approaches zero when going away from the surface deep into the bulk or vacuum, at which points z_1 and z_2 are chosen. However, for atomically-thin MXenes, z_1 is not well defined because of the non-zero $\Delta\rho$ in the bulk (see Fig. S1). This invalidates the use of Eq. (2). Albeit this ambiguity, the dipole effect can still be approximated by the dipole moment density of the MXene with only one side of the surfaces terminated, which we calculate as:

$$\Delta D_s \sim D_s = \int_{z1}^{z2}\iint z\rho(x,y,z)\mathrm{d}x\mathrm{d}y/S$$

where z_1 and z_2 are chosen at the points where $\rho = 0$ (i.e. deep into vacuum).

Fig. 2b plots the ΔW as a function of D_s. We find that ΔW always has the same sign as D_s, suggesting that D_s controls the decrease or increase of W. Specifically, O termination always leads to a positive D_s (i.e. the negative end of the dipole points to T), OH termination always results in a negative D_s, while F can have either positive or negative D_s depending on the specific material

Indeed, this matches well with the decrease or increase in W. Note that the surface OH group itself has a dipole moment ~ -0.33 eÅ with O pointing to the M, which is compensated by an opposite dipole due to the charge redistribution induced by OH adsorption; nevertheless, the net dipole moment is still negative. We also note that the negative dipole of F termination for some materials does not mean that F carries positive charge. As shown by the electron density change in Fig. S1, after F adsorption, the surface M layer transfers electrons to both F and the underneath X layer; however, X gets more electrons than T, resulting in a negative dipole even when F is negatively charged. Compared with F, O tends to get more electrons to saturate the two unpaired p orbitals. The amount of electron transfer from M to O is greater than that to X, thus the O induced dipole is always positive. These arguments explain well the relationships between surface termination and the W change as mentioned above.

More quantitatively, for O or F terminated MXenes, the magnitude of ΔW and D_s exhibit a quasi-linear correlation, but for OH there is no clear correlation. Similar observation has been reported in Ref. [27]. This is probably due to the complexity of the OH terminated surface, where the dipole is contributed by both the OH group itself and the adsorption-induced charge redistribution. In addition, the ΔE_F can vary with M, reducing the correlation between ΔW and D_s.

The high/low W of some of the MXenes suggests that they have the potential of injecting carriers into 2D semiconductors. One of the most important parameters that determine the resistance to carrier injection is the Schottky barrier height (Φ), which is defined as the energy difference between the Fermi level and the band edge of the semiconductor in the MSJ:

$$\Phi_e = E_{CBM} - E_F,\ \Phi_h = E_F - E_{VBM} \quad (3),$$

where Φ_e and Φ_h are the Schottky barrier heights for electrons and holes, respectively; CBM denotes the conduction band minimum of the semiconductor, and VBM denotes the valence band maximum. To reduce the contact resistance and improve device performance, Φ_e (for electron injection) or Φ_h (for hole injection) needs to be as low as possible (a SB-free contact is achieved when Φ becomes zero or negative). For a defect-free MSJ, neglecting the interaction between the metal and the semiconductor, Eq. (3) becomes:

$$\Phi_e = E^0_{CBM} + W,\ \Phi_h = -W - E^0_{VBM} \quad (4),$$

where E^0_{CBM} and E^0_{VBM} are the CBM and VBM energies of the semiconductor in vacuum. Therefore a low/high W is beneficial for electron/hole injection. Although Eq. (4) provides general guidance for comparing Φ, the metal-semiconductor interaction usually causes deviations of (4) from (3),[29] thus the accurate assessment of Φ requires explicit modeling or measurement of the heterogeneous MSJ.

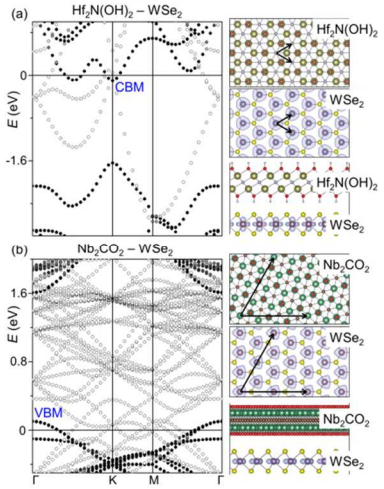

Figure 3. Band structures (left) and atomic structures (right), for: (a) the $Hf_2N(OH)_2$-WSe_2 junction; (b) the Nb_2CO_2-WSe_2 junction. The Fermi level is set to zero. The WSe_2 contribution to the electronic state is represented by the blackness of the circle interior (i.e. full black means the state is purely from WSe_2, full white indicates the state is purely from the MXene, while gray suggests the state is hybridized between WSe_2 and MXene). The charge density distributions of WSe_2 CBM in the $Hf_2N(OH)_2$-WSe_2 junction and WSe_2 VBM in the Nb_2CO_2-WSe_2 junction are displayed by the light-blue iso-surfaces on the right. The arrows show the periodic cells that are overlaid in the junctions.

As an example, Figure 3a shows a MSJ with $Hf_2N(OH)_2$ on top of WSe_2. These two materials have a small lattice mismatch of <3%, thus the primitive cells (marked by arrows) are used for calculation. To determine the band edge positions of semiconductor in the MSJ, we analyze the character of the electronic state by projecting its wavefunction onto each atom (this method has been widely used for studying SB[30, 31]). The WSe_2 contribution to the state is reflected by the color of the circle in the band structure. We find that the Fermi level of the MSJ is above the CBM (which is confirmed by the charge density distribution), showing a negative Φ_e, i.e. electrons are spontaneously transferred from $Hf_2N(OH)_2$ to the conduction band of WSe_2 upon contact. Note that Fig. 3a is calculated using PBE functional (with the D3 method for vdW correction), which is known to underestimate the band gap. To check whether this affects the Φ_e, we re-calculated the electronic structure using B3PW91 hybrid functional, which generally gives much more accurate band gaps[32, 33] as well as band offsets[34]. As shown in the SI, the Φ_e remains negative (-0.10 eV for PBE vs. -0.12 eV for B3PW91). Therefore, we conclude that $Hf_2N(OH)_2$ spontaneously injects electrons into WSe_2 upon contact. Since WSe_2 has the highest CBM among the commonly studied 2D semiconductors (molybdenum/tungsten dichalcogenides and black phosphorus)[35, 36], while $Hf_2N(OH)_2$ has the highest W among OH terminated MXenes (Fig. 1a), we expect that all the OH terminated MXenes can form SB-free contacts for electron injection into these common 2D semiconductors.

Fig. 3b shows a MSJ with Nb_2CO_2 on top of WSe_2. These two materials have a large lattice mismatch of >5%, thus we used a supercell (marked by arrows) for calculation in order to minimize the strain. Analogous to the above case, we find that the Fermi level is below the VBM of the semiconductor in the MSJ, showing a negative Φ_h, i.e. holes are spontaneously transferred from Nb_2CO_2 to the valance band of WSe_2 upon contact. The negative Φ_h is confirmed by using the B3PW91 hybrid functional to recalculate the electronic structure (-0.10 eV for PBE vs. -0.08 eV for B3PW91; see SI). We note that many other O-terminated MXenes have a W higher than that of Nb_2CO_2, so that they can also be expected to exhibit even more negative Φ_h. In addition, the spin-orbit coupling (SOC) further increases the VBM[35] and hence reduce the Φ_h (similarly, the SOC generally decreases the CBM and thus also reduce the Φ_e, while for 2D transition metal dichalcogenides, the SOC has negligible effect on the CBM position[35]). Therefore, we conclude that SB-free contacts for hole injection into WSe_2 can be formed by using Nb_2CO_2, V_2CO_2, Cr_2CO_2, Mo_2CO_2, $Ti_3C_2O_2$, $V_3C_2O_2$, $Ti_4C_3O_2$, $V_4C_3O_2$, Ti_2NO_2, V_2NO_2, and $Ti_4N_3O_2$.

The ability to achieve SB-free contacts by using 2D MXenes is due to not only their low/high W of specific materials, but also the weak vdW interactions between the metal and the semiconductor in the MSJ, which has been shown to reduce the Fermi level pinning effect[16]. This is also observed in our examples: although Nb_2CO_2 and Pt have a similar W (Fig. 1a), the Nb_2CO_2 has a negative Φ_e as shown in Fig. 3b, while the Φ_e for Pt is calculated to be ~ 0.34 eV[37] (both cases are calculated at the PBE level without SOC), confirming a weaker Fermi level pinning at the vdW MSJ.

In current experiments, MXenes are usually terminated with a mixture of F, O, and OH, due to the use of aqueous F-containing solution for etching. The mix of O and OH at the surface brings the W back into an intermediate value. Therefore we consider it best to have only one type dominant. Although in some cases F termination can also lead to a low/high W (e.g. Mo_2CF_2, $V_3C_2F_2$, $V_4C_3F_2$, Hf_2NF_2; see Fig. 1a), it generally results in a modest W, suggesting that F termination should be suppressed in most cases. Experimentally, it has been shown that using LiF-HCl instead of HF can increase/decrease the ratio of O/F[38], and alkalization treatment can increase the concentration of OH[13]. Here we show that the preference of different terminations can be further modified by applying an electrochemical potential. The formation free energy (ΔG_T) of T termination with respect to bare surface can be calculated as:

$$\Delta G_T = G(M_{n+1}X_nT_2) - G(M_{n+1}X_n) - 2G(T)$$

where $G(H) = 1/2G(H_2) - eU$, $G(OH) = G(H_2O) - G(H)$, $G(O) = G(H_2O) - 2G(H)$. $G(H_2)$ and $G(H_2O)$ are the free energies of H_2 and H_2O at standard condition, respectively, and U is the applied voltage vs. the reversible hydrogen electrode (RHE). For simplicity, we assume that the system is also in equilibrium with HF at standard condition, thus: $G(F) = G(HF) - G(H)$ (Note this assumption overestimates the $G(F)$).

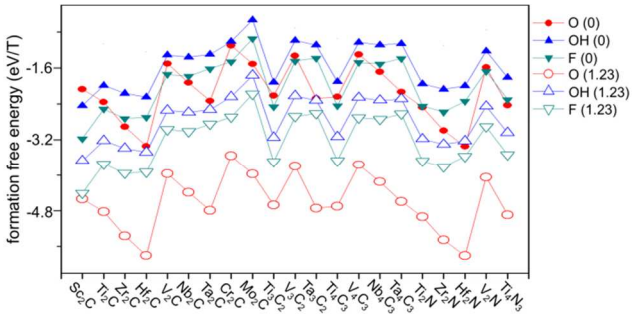

Figure 4. The calculated formation free energies of surface terminations for various MXenes (see the main text for definition), at U = 0 (solid) and 1.23 V (hollow) vs. RHE.

Figure 4 shows the calculated ΔG_T at U = 0 and 1.23 V, which correspond to the thermodynamic limits for water splitting. We find that F termination is always more favorable thermodynamically than OH (ΔG_F and ΔG_{OH} exhibit a notable positive correlation), while the preference of F vs. O depends on the specific material and the U. At U = 1.23 V, O termination becomes much more favorable than F (> 0.8 eV/T; except Sc_2C). This benefits from the stronger dependence of ΔG_O on U compared to ΔG_F, since the adsorption of O involves more charge transfer. Therefore, a high U thermodynamically favors O termination. Starting from O terminated MXenes, one can convert the surface to OH termination by applying a positive U, as the difference between ΔG_O and ΔG_{OH} becomes smaller with increasing U and can be inverted given a high enough U (see the SI for the assessment of the critical U for the case of V_2C). Moreover, treating MXenes with O/H gas or plasma could also modify the surface towards the desired terminations.

There are other benefits of using 2D MXenes as metal electrodes. Because of the atomic thickness, the 2D metals are transparent and flexible[39, 40], thus they can be integrated into transparent and flexible electronics.[14, 41-43] It also allows for full encapsulation of the device by boron nitride to avoid material contamination/degradation[44, 45]. Moreover, the atomically-flat interface between the metal and the semiconductor, and the suppression of gap states at the interface due to the weak vdW interaction[16], can

reduce the charge carrier scattering and recombination, improving the performance for electronic and optoelectronic applications. As a final note, we point out that defects in the semiconductors often create gap states[46] that lead to the Fermi level pinning, and would cause deviation from the calculated SB values. However, this effect is similar for different metal contacts. Therefore, it is robust to conclude that, compared with other metals, the use of proper MXenes can lower the SB.

In summary, based on first-principles calculations, we demonstrate the potential of surface-engineered MXenes as SB-free contacts to 2D semiconductors. The work functions of MXenes show strong dependence on the surface termination, which is largely due to the surface dipole effect. When forming vdW contact with 2D semiconductors, some of O terminated MXenes can spontaneously inject holes, while all the OH terminated MXenes can spontaneously transfer electrons. We also suggest synthetic routes towards the desired surface terminations.

ASSOCIATED CONTENT

Supporting Information

The Supporting Information is available free of charge on the ACS Publications website. Stacking order of the group-6 MXenes; Electron redistribution upon surface termination; Verification of SB-free contacts for electron/hole injection by the hybrid functional B3PW91, The stability of O and OH termination of V2C under applied potentials; Table for the data used in Figs, including the work function, surface dipole moment density, and formation free energies.

AUTHOR INFORMATION

Corresponding Author

yuanyue.liu.microman@gmail.com
wag@wag.caltech.edu, ORCID:0000-0003-0097-5716

Notes

The authors declare no competing financial interests.

ACKNOWLEDGMENT

Y.L. thanks the support from Resnick Prize Postdoctoral Fellowship at Caltech. This research was funded by DOE DE-SC0014607. This work used computational resources sponsored by the DOE's Office of Energy Efficiency and Renewable Energy and located at the National Renewable Energy Laboratory; the Extreme Science and Engineering Discovery Environment (XSEDE; supported by NSF Grant ACI-1053575); and the National Energy Research Scientific Computing Center (NERSC; a DOE Office of Science User Facility supported by the Office of Science of the U.S. DOE under Contract DE-AC02-05CH11231).

REFERENCES

1. Lei, J.-C.; Zhang, X.; Zhou, Z. *Frontiers of Physics* **2015,** 10, 276-286.
2. Naguib, M.; Mochalin, V. N.; Barsoum, M. W.; Gogotsi, Y. *Adv. Mater.* **2014,** 26, 992-1005.
3. Naguib, M.; Kurtoglu, M.; Presser, V.; Lu, J., et al. *Adv. Mater.* **2011,** 23, 4248-4253.
4. Eklund, P.; Beckers, M.; Jansson, U.; Högberg, H., et al. *Thin Solid Films* **2010,** 518, 1851-1878.
5. Ghidiu, M.; Lukatskaya, M. R.; Zhao, M.-Q.; Gogotsi, Y., et al. *Nature* **2014,** 516, 78-81.
6. Tang, Q.; Zhou, Z.; Shen, P. *J. Am. Chem. Soc.* **2012,** 134, 16909-16916.
7. Xie, Y.; Naguib, M.; Mochalin, V. N.; Barsoum, M. W., et al. *J. Am. Chem. Soc.* **2014,** 136, 6385-6394.
8. Naguib, M.; Halim, J.; Lu, J.; Cook, K. M., et al. *J. Am. Chem. Soc.* **2013,** 135, 15966-15969.
9. Liang, X.; Garsuch, A.; Nazar, L. F. *Angew. Chem. Int. Ed.* **2015,** 54, 3907-3911.
10. Lukatskaya, M. R.; Mashtalir, O.; Ren, C. E.; Dall'Agnese, Y., et al. *Science* **2013,** 341, 1502-1505.
11. Boota, M.; Anasori, B.; Voigt, C.; Zhao, M.-Q., et al. *Adv. Mater.* **2016,** 28, 1517-1522.
12. Rasool, K.; Helal, M.; Ali, A.; Ren, C. E., et al. *ACS Nano* **2016,** 10, 3674-3684.
13. Peng, Q.; Guo, J.; Zhang, Q.; Xiang, J., et al. *J. Am. Chem. Soc.* **2014,** 136, 4113-4116.
14. Fiori, G.; Bonaccorso, F.; Iannaccone, G.; Palacios, T., et al. *Nat. Nanotechnol.* **2014,** 9, 768-779.
15. Allain, A.; Kang, J.; Banerjee, K.; Kis, A. *Nat. Mater.* **2015,** 14, 1195-1205.
16. Liu, Y.; Stradins, P.; Wei, S.-H. *Science Advances* **2016,** 2.
17. Xu, J.; Shim, J.; Park, J.-H.; Lee, S. *Advanced Functional Materials* **2016,** 26, 5328-5334.
18. Liu, Y.; Weiss, N. O.; Duan, X.; Cheng, H.-C., et al. *Nature Reviews Materials* **2016**, 16042.
19. Novoselov, K. S.; Mishchenko, A.; Carvalho, A.; Castro Neto, A. H. *Science* **2016,** 353.
20. Kresse, G.; Hafner, J. *Phys. Rev. B* **1993,** 47, 558-561.
21. Kresse, G.; Furthmüller, J. *Phys. Rev. B* **1996,** 54, 11169-11186.
22. Kresse, G.; Joubert, D. *Phys. Rev. B* **1999,** 59, 1758-1775.
23. Blöchl, P. E. *Phys. Rev. B* **1994,** 50, 17953-17979.
24. Perdew, J. P.; Burke, K.; Ernzerhof, M. *Phys. Rev. Lett.* **1996,** 77, 3865-3868.
25. Becke, A. D. *J. Chem. Phys.* **1993,** 98, 5648-5652.
26. Grimme, S.; Antony, J.; Ehrlich, S.; Krieg, H. *J. Chem. Phys.* **2010,** 132, 154104.
27. Khazaei, M.; Arai, M.; Sasaki, T.; Ranjbar, A., et al. *Phys. Rev. B* **2015,** 92, 075411.
28. Das, S.; Chen, H.-Y.; Penumatcha, A. V.; Appenzeller, J. *Nano Lett.* **2012,** 13, 100-105.
29. Tung, R. T. *Applied Physics Reviews* **2014,** 1, 011304.
30. Gong, C.; Colombo, L.; Wallace, R. M.; Cho, K. *Nano Lett.* **2014,** 14, 1714-1720.
31. Kang, J.; Liu, W.; Sarkar, D.; Jena, D., et al. *Phys. Rev. X* **2014,** 4, 031005.
32. Xiao, H.; Tahir-Kheli, J.; Goddard, W. A. *J. Phys. Chem. Lett.* **2011,** 2, 212-217.
33. Crowley, J. M.; Tahir-Kheli, J.; Goddard, W. A. *J. Phys. Chem. Lett.* **2016,** 7, 1198-1203.
34. Xiao, H.; Goddard, W. A. *J. Chem. Phys.* **2014,** 141, 094701.
35. Kang, J.; Tongay, S.; Zhou, J.; Li, J., et al. *Appl. Phys. Lett.* **2013,** 102, 012111.
36. Cai, Y.; Zhang, G.; Zhang, Y.-W. *Scientific Reports* **2014,** 4, 6677.
37. Wang, Y.; Yang, R. X.; Quhe, R.; Zhong, H., et al. *Nanoscale* **2015**.
38. Hope, M. A.; Forse, A. C.; Griffith, K. J.; Lukatskaya, M. R., et al. *Phys. Chem. Chem. Phys.* **2016,** 18, 5099-5102.
39. Dillon, A. D.; Ghidiu, M. J.; Krick, A. L.; Griggs, J., et al. *Advanced Functional Materials* **2016,** 26, 4162-4168.
40. Hantanasirisakul, K.; Zhao, M.-Q.; Urbankowski, P.; Halim, J., et al. *Advanced Electronic Materials* **2016,** 2, 1600050-n/a.
41. Akinwande, D.; Petrone, N.; Hone, J. *Nat Commun* **2014,** 5.
42. Das, S.; Gulotty, R.; Sumant, A. V.; Roelofs, A. *Nano Lett.* **2014,** 14, 2861-2866.
43. Roy, T.; Tosun, M.; Kang, J. S.; Sachid, A. B., et al. *ACS Nano* **2014,** 8, 6259-6264.
44. Cui, X.; Lee, G.-H.; Kim, Y. D.; Arefe, G., et al. *Nat. Nanotechnol.* **2014,** 10, 534–540.
45. Avsar, A.; Vera-Marun, I. J.; Tan, J. Y.; Watanabe, K., et al. *ACS Nano* **2015,** 9, 4138-4145.
46. Liu, Y.; Stradins, P.; Wei, S.-H. *Angew. Chem. Int. Ed.* **2016,** 55, 965-968.

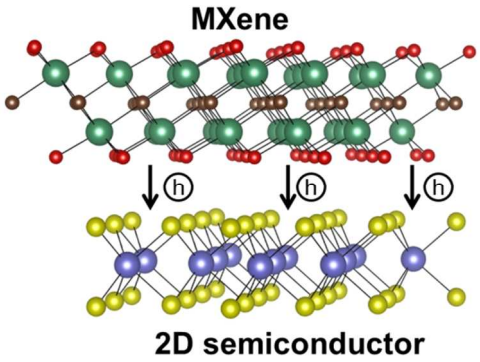
MXene
h
h
h
2D semiconductor